

On the pulsation modes of OGLE small amplitude red giant variables in the LMC

Masaki Takayama^{*}, Hideyuki Saio and Yoshifusa Ita

Astronomical Institute, Graduate School of Science, Tohoku University, Sendai, Miyagi 980–8578, Japan

ABSTRACT

We discuss the properties of pulsations in the OGLE Small Amplitude Red Giants (OSARGs) in the Large Magellanic Cloud (LMC). We consider stars below the red-giant tip in this paper. They are multi-periodic and form three sequences in the period-luminosity plane. Comparing the periods and period ratios with our theoretical models, we have found that these sequences correspond to radial first to third overtones, and nonradial dipole p_4 and quadrupole p_2 modes. The red-giant branch stars of OSARGs consist of stars have initial masses of $\sim 0.9 - 1.4M_{\odot}$ which corresponds to a luminosity range of $\log L/L_{\odot} \simeq 2.8 - 3.4$. With these parameters, the scaled optimal frequency ν_{\max} for solar-like oscillations goes through roughly the middle of the three sequences in the period-luminosity plane, suggesting the stochastic excitation is likely the cause of the pulsations in OSARGs.

Key words: stars:evolution – stars:late-type – stars:oscillations – stars:variables – Magellanic Clouds

1 INTRODUCTION

Recently, the number of known long period variables (LPVs) has increased dramatically thanks to the analyses for the extensive photometric data from various gravitational microlensing surveys, Massive Compact Halo Object (MACHO), Optical Gravitational Lensing Experiment (OGLE), Expérience de Recherche d’Objets Sombres (EROS), and Microlensing Observations in Astrophysics (MOA) (e.g., Wood et al 1999; Cioni et al. 2001; Kiss & Bedding 2003; Soszyński et al. 2004; Ita et al. 2004; Noda et al. 2004).

Analyzing photometric data of red giants brighter than $\log L/L_{\odot} \sim 2.7$ in MACHO survey of the LMC, Wood et al (1999) found several sequences in the period-luminosity (PL) plane with periods ranging from about 20 to a thousand days. They named these sequences A, B, C, E, and D from shorter to longer periods, in which the sequence C coincides with the known PL relation of Mira variables. Later Ita et al. (2004) found that sequence C’ which corresponds to overtone Mira variables can be isolated from the sequence B. From the light curves, sequence E is attributed to eclipsing binaries (Wood et al 1999; Nicholls, Wood & Cioni 2010). Sequence D is sometimes called Long Secondary Periods (LSPs) because in those stars, shorter period pulsations are superposed on a LSP of about 400 – 1500 days. Although the origin of the sequence D is discussed by several authors, it is not settled yet (A historical account on LPVs is given

in e.g., Soszyński et al. 2004, 2007). In this paper we do not consider stars on sequence D.

Soszyński et al. (2004) isolated OGLE small amplitude red giants (OSARGs) from the LPVs. The OSARGs can be divided into two groups; red-giant branch (RGB) stars less luminous than the giant tip (corresponding to the occurrence of the core helium flash) and asymptotic giant branch (AGB) stars. Soszyński et al. (2004) identified three ridges in the PL plane for the RGB OSARGs named b_1 , b_2 and b_3 from longer to shorter periods; b_2 and b_3 apparently correspond to sequence B and A of Wood et al (1999), and B^- and A^- of Ita et al. (2004), respectively. Furthermore, b_1 , b_2 and b_3 correspond to R_1 , R_2 , and R_3 discussed by Kiss & Bedding (2003) from OGLE-II data. Similarly, Soszyński et al. (2004) named four AGB OSARGs as a_1 , a_2 , a_3 and a_4 . In this paper we determine pulsation modes of the RGB OSARGs (i.e., b_1 , b_2 and b_3 sequences) in the LMC.

2 OBSERVATIONAL PROPERTIES OF RGB OSARGS

We use periods of RGB OSARGs in the LMC given in the OGLE-III catalog (Soszyński et al. 2009), in which up to three periods are listed for each star. In the period-luminosity plane, OSARGs are known to form several sequences. We adopt the nomenclature of the sequences and the way of selecting RGB OSARGs introduced by Soszyński et al. (2004); the sequences of RGB OSARGs are named b_1 , b_2 , and b_3 .

^{*} E-mail:m.takayama@astr.tohoku.ac.jp

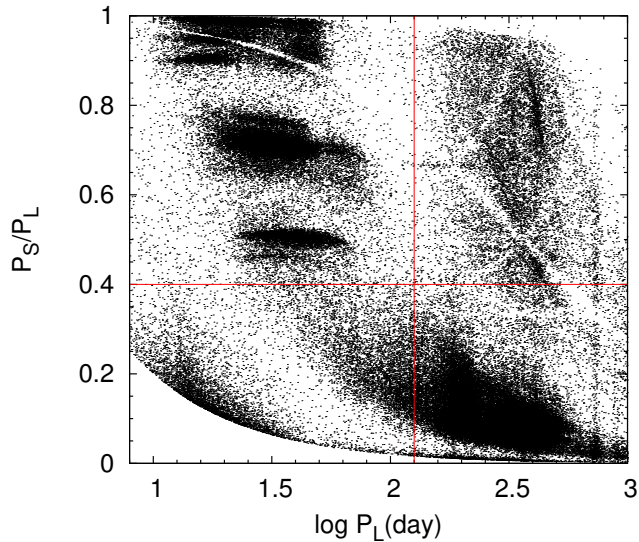


Figure 1. All the periods of RGB OSARGs in the catalog of OGLE-III OSARGs by Soszyński et al. (2009) are plotted in the Period vs period-ratio plane (Petersen diagram). The ordinate indicates the ratio of the shorter (P_S) to the longer period (P_L) for each period pair, and the abscissa the logarithmic value of the longer period. Vertical and horizontal lines are used to exclude stars having periods belong to the sequence D (or LSPs).

Figure 1 shows a Petersen (period vs period-ratio) diagram for all the RGB OSARGs (about 45,500) in the OGLE-III catalog. In this diagram (and in similar ones shown below), the ordinate indicates the ratio of the shorter to the longer period of a period pair, P_S/P_L , and the abscissa indicates the logarithmic value of the longer period, $\log P_L$. Because each star has three periods, each star appears three times in this diagram. In this figure we see a big dense group in the lower right corner. The group is formed by the stars associated with the long period sequence D; i.e. stars having long secondary periods (LSPs). The origin of their long periodicity is not clear yet, but majority of them seem to be irrelevant (or unrelated) to stellar pulsation (e.g., Nicholls et al. 2009; Soszyński 2007; Wood et al. 2004).

In this paper we do not discuss LSPs. To exclude the stars having LSPs from the sample, we have drawn a horizontal line at $P_S/P_L = 0.4$, and a vertical line at $\log P_L = 2.1$ in Fig. 1, and we have selected stars located only in the upper-left quadrant in this figure. After excluding stars with LSPs, we have a set of about 8,500 RGB OSARGs in the LMC.

The selected stars are plotted in the period-luminosity plane in Fig. 2, where the ordinate adopts the reddening free Wesenheit index

$$W_I = I - 1.55(V - I) \quad (1)$$

with I and V mean magnitudes. In this period-luminosity diagram we see three obvious sequences (or ridges). They are b_1 , b_2 , and b_3 sequences from longer to shorter periods, adopting the nomenclature defined by Soszyński et al. (2004). We note that the sequence D is clearly removed from our sample. For the LMC, $W_I \approx 11[mag]$ corresponds to

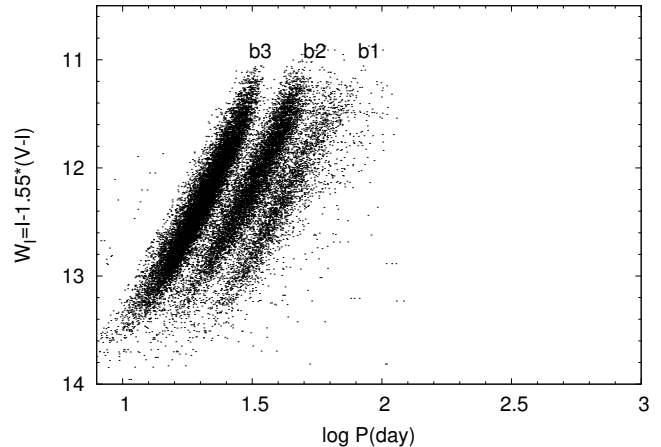


Figure 2. Period- W_I diagram for our selected sample of RGB OSARGs (stars having LSPs are removed), where W_I is the reddening free Wesenheit index defined by equation (1). Three ridges are named b_1 , b_2 , and b_3 (from longer to shorter periods) following the nomenclature introduced by Soszyński et al. (2004)

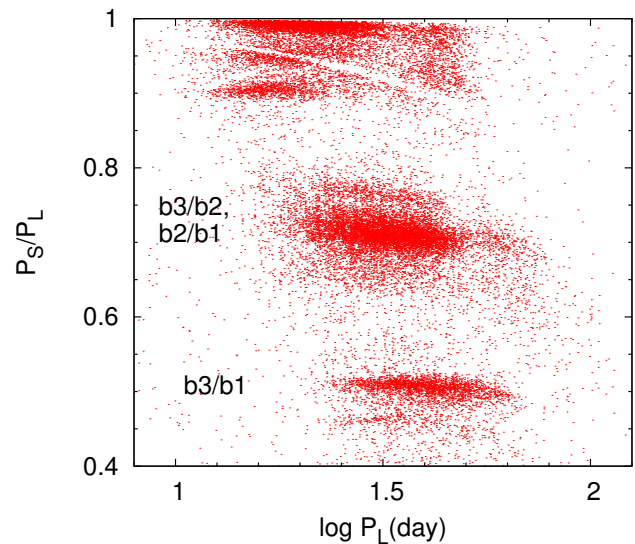


Figure 3. Period/Period-ratio (Petersen) diagram for our sample of RGB OSARGs (red dots), from which LSPs (sequence D) are removed. This diagram corresponds to the top-left quadrant of Fig. 1. Period-ratios of about 0.5 are produced by the ratios of b_3/b_1 , while ratios of about 0.7 can be attributed to b_2/b_1 and b_3/b_2 . The ridges above ~ 0.9 indicates the presence of nonradial pulsations.

the giant tip at $\log L/L_\odot \approx 3.4$, while $W_I \approx 11[mag]$ corresponds to $\log L/L_\odot \approx 2.8$.

Figure 3 shows the Petersen diagram for our selected stars. This figure is the same as the top-left quadrant of Fig. 1. We note that despite a significant reduction in the number of stars by excluding LSPs, the property of the distribution in the Petersen diagram is unchanged. The structure of the distribution is more clearly seen in Fig. 3. We see two major ridges in Fig. 3 at $P_S/P_L \approx 0.5$ and ≈ 0.7 ; the former corresponds to the period ratios between b_3 and b_1 ,

and the latter is formed by the ratios b_2/b_1 and b_3/b_2 . The additional ridges at $P_S/P_L \approx 0.90$ and ≈ 0.95 are attributed to the presence of sub-ridges in the P-L plane along b_2 and b_3 as discussed by Soszyński et al. (2007). The less densely populated ridges in Fig. 3 at $P_S/P_L \approx 0.45$ and ≈ 0.75 might be associated with the sub-ridges of b_2 and b_3 . These sub-ridges strongly suggest the presence of nonradial pulsations in OSARGs.

We note that the Petersen diagram (Fig. 3) has an advantage over the period-luminosity diagram such as Fig. 2 in comparing theoretical results with observation to determine pulsation modes. Obviously the PL diagram is affected by errors in luminosities and stellar radii, while only the accuracy in periods for each star matters in the Petersen diagram. Therefore, we use Petersen diagrams to determine pulsation modes for the period-luminosity sequences, b_1 – b_3 .

3 MODELS

In order to identify pulsation modes for each of the corresponding OSARG(RGB) PL relations, we have calculated linear nonadiabatic radial and non-radial pulsation periods for envelope models along evolutionary tracks. The evolutionary models were calculated by using the MESA stellar evolution code (Paxton et al. 2011) for initial masses of 0.9, 1.0, 1.1, 1.2, 1.3, 1.4 and $1.6M_\odot$, in which wind mass loss is included by adopting Reimers’ formula (Reimers 1975)

$$\dot{M} = -4 \times 10^{-13} \eta \frac{(L/L_\odot)(R/R_\odot)}{(M/M_\odot)} M_\odot \text{ yr}^{-1} \quad (2)$$

with $\eta = 0.4$. For our canonical models, we have adopted a chemical composition of $(X, Z) = (0.71, 0.01)$ and a mixing-length of 1.5 pressure scale height. (We discuss the effects of changing these parameters later in this paper.) Opacity tables of OPAL (Iglesias & Rogers 1996) with low-temperature extension by Alexander & Ferguson (1994) were used.

Envelope models for radial and nonradial pulsation analyses were calculated at selected evolutionary stages of each evolutionary track. We set the surface boundary at $\tau=0.001$ for the envelope calculations with τ being the optical depth associated with the Rosseland-mean opacity. Fox & Wood (1982) discussed the uncertainties in the pulsation properties caused by various assumptions around the outer boundary of AGB models. To check the influence of the particular place of the outer boundary, we have calculated models imposing the outer boundary condition at $\tau=0.01$. We have found that the difference in periods is less than a few percent, and that the period ratios are hardly different. For radial pulsations we set the bottom of an envelope arbitrarily at $r/R \sim 1/100$. For nonradial pulsations we set the inner boundary just below the convective envelope, suppressing possible coupling with high order core g-modes. This is justified because only p-modes completely trapped in the convective envelope can be excited to observable amplitudes (e.g., Dupret et al. 2009).

Linear nonadiabatic analyses for radial and nonradial pulsations were performed using the codes described in Saio, Winget, & Robinson (1983) and Saio & Cox (1980), respectively. In both cases convection-pulsation coupling is

disregarded by neglecting the perturbation of the divergence of the convective flux. Convective turnover time in the convective envelope of a typical model for RGB OSARGs varies from much longer (deep interior) to shorter (in the outer layers) than low-order pulsation periods. This indicates that we should not trust the stability results of our analyses. For this reason we used only periods from these codes disregarding the stability results. We compared our periods and period ratios with Fig.3 of Xiong & Deng (2007), in which the effect of convection-pulsation interaction is included, and found our results to be consistent with their values. This confirms that the convection-pulsation coupling hardly affects periods, and justifies the use of our theoretical periods. This is understandable because the nonadiabaticity is not very strong in the RGB models and the nonadiabatic periods are very close to the adiabatic ones. Finally, the fact that the convective turnover time is comparable to the pulsation periods in some layers in the envelope is favorable for the pulsations to be stochastically excited by turbulent convection.

4 COMPARISON WITH OBSERVATIONS

4.1 Mode identifications

The period of a pulsation mode is approximately proportional to $1/\sqrt{\bar{\rho}}$ with $\bar{\rho}$ being the mean density (e.g., Cox 1980), which depends on the stellar mass and radius. Generally the dependence of the periods ratios on these two parameters is rather weak. In addition, Fig. 3 indicates the period ratios depend only weakly on period. For that reason, the period ratios are useful for determining pulsation modes, while pulsation periods are used to determine the appropriate luminosity (or mass) ranges.

First, we determine which radial modes are excited in the RGB OSARGs. Figs. 4 and 5 compare observed period ratios with theoretical ones formed by the radial fundamental (F), 1st (1O), 2nd (2O), and 3rd (3O) overtone periods along a part of the evolutionary track ($2.7 \leq \log L/L_\odot \leq 3.35$) of an initial mass of $1.1M_\odot$. The luminosity range roughly corresponds to that of RGB OSARGs. Fig. 4 shows the ratios involving fundamental mode (denoted as ‘F’). Obviously none of the period ratios involving the fundamental mode agrees with any major ridges around 0.5 or 0.7. This indicates that the fundamental mode is not responsible for any of the period-luminosity sequences, b_1 , b_2 , and b_3 . For this reason we do not consider the radial fundamental mode any further.

Fig. 5 shows that the ratio of the third overtone to the first overtone (3O/1O) is close to 0.5 in the middle of the luminosity range agreeing with the b_3/b_1 ratio. In addition, the period ratios of 2O/1O and 3O/2O are around 0.7 in the middle of the luminosity range, although they do not go through the central part of the ridge. From these comparisons we conclude that the radial first, second, and third overtones correspond to, respectively, the b_1 , b_2 , and b_3 sequences of the RGB OSARGs. We note that Dziembowski & Soszyński (2010) was unable to explain the period-luminosity sequences b_2 and b_3 by assigning the first overtone (1O) to b_2 and the second overtone (2O) to b_3 . Our identifications differ by one order; i.e., 2O to b_2 and 3O to b_3 .

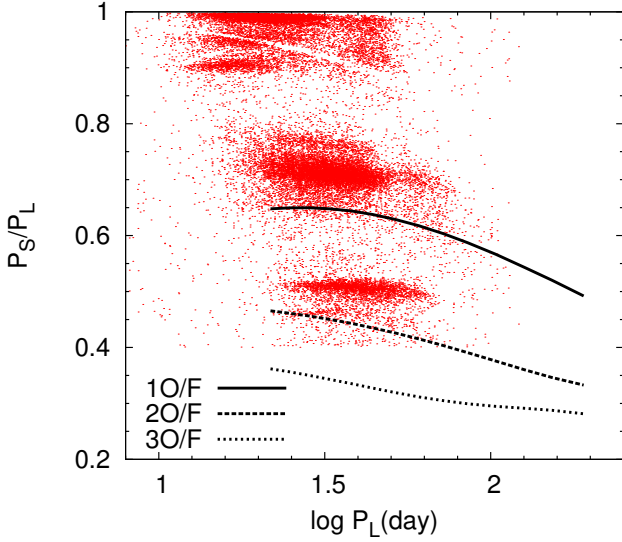


Figure 4. Period ratios of the first (1O), second (2O) and third overtone (3O) modes to the radial fundamental mode (F) for our $1.1M_{\odot}$ models are compared to the observed ratios of OSARGs in the LMC (red dots). The solid line shows the first overtone to fundamental period ratio (1O/F), while the dashed line is for the 2O/F ratio and the dotted line is for the 3O/F ratio. These lines do not fit with any of the ridges in the distribution of OSARG period ratio, indicating that fundamental mode are not excited in the RGB OSARGs.

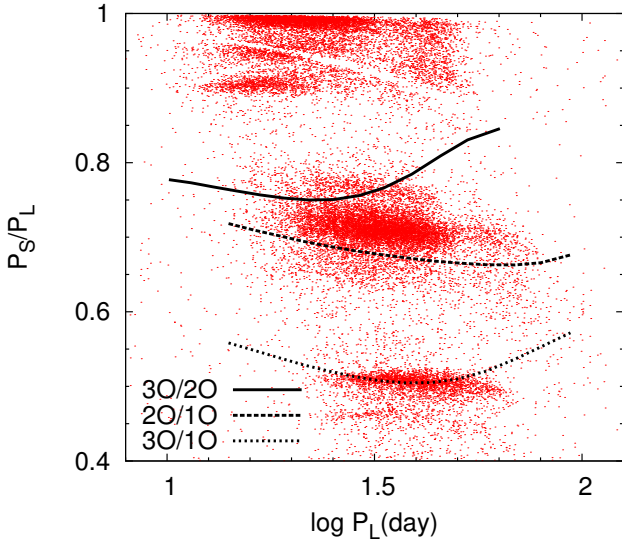


Figure 5. The same as 4 but for period ratios without fundamental mode. The solid, dashed and dotted lines show the ratios between radial overtones as indicated. The 3O/2O and 2O/1O ratios go through close to the ridge around 0.7, while the 3O/1O ratio goes through the ridge at 0.5.

Fig. 5 indicates that the theoretical relations of $1.1M_{\odot}$ models cannot explain the period ratios for the whole period range of the RGB OSARGs. They agree with the observed ratios only in a period range of $1.5 \lesssim \log P(1O) \lesssim 1.7$ which corresponds to a luminosity range of $3.0 \lesssim \log L/L_{\odot} \lesssim 3.15$. This means that we have to apply models having different initial masses for different luminosity (hence period) ranges. In other words, the running of the PL relations must be explained by not the stellar evolution of a single mass star, but the evolution of stars with a range of initial masses. We will discuss different mass models in the next subsection.

Here, we consider period ratios involving nonradial pulsations in our $1.1M_{\odot}$ models in the luminosity range $3.0 \lesssim \log L/L_{\odot} \lesssim 3.15$. Figs. 6 and 7 show period ratios between dipole ($l = 1$) and radial modes, and quadrupole ($l = 2$) and radial modes, respectively, where solid lines, lines with triangles, lines with filled circles correspond to the ratios with 1O, 2O, 3O, respectively. Nonradial modes considered are $p_1 \dots p_4$ for both $l = 1$ and 2.

Fig. 6 indicates that among the dipole modes, only p_4 is consistent with all the observed ridges in the Petersen diagram. This mode explains the $P_S/P_L \approx 0.45$ sub-ridge by paring with 1O (b_1), the ≈ 0.7 major ridge by paring with 2O (b_2), and $\approx 0.9 - 0.95$ by paring with 3O (b_3). Therefore, we can identify the dipole ($l = 1$) p_4 -mode as a sub-ridge of b_3 .

Fig. 7 indicates that for the quadrupole ($l = 2$) modes, p_2 -mode yields period ratios consistent with the observed ones; ratios with O1 and O3 correspond to the central ridge at ≈ 0.7 and the ratio with O2 corresponds to the ridge at ≈ 0.95 . This means that quadrupole p_2 -mode corresponds to a sub-ridge of b_2 . This figure might also indicate the possible presence of $p_1(l = 2)$ as a sub-ridge of b_1 . More data are needed to confirm its presence.

In summary, we have identified 1O for b_1 , 2O and $p_2(l = 2)$ for b_2 , and 3O and $p_4(l = 1)$ for b_3 . Soszyński et al. (2007) argued that each of the sequences b_2 and b_3 has two sub-ridges in addition to a main ridge, while our mode identifications explain only one sub- and main ridge pair. Second sub-ridges, if real, might correspond to higher degree ($l \geq 3$) modes. Also, the ratios with the second sub-ridge within each of sequences b_2 and b_3 might be consistent with the period ratios around 0.98 (e.g., Fig. 7) which we cannot explain with our mode identifications. It is interesting that the main part of the ridge at $P_S/P_L \approx 0.7$ is reproduced by the ratios involving nonradial pulsations. This might indicate that main relations of b_2 and b_3 sequences are formed by nonradial pulsations; $p_2(l = 2)$ and $p_4(l = 1)$, respectively, rather than radial modes.

4.2 Mass ranges

In the previous subsection we found that radial 1O, 2O, and 3O, and nonradial $p_4(l = 1)$ and $p_2(l = 2)$ modes are consistent with the observed period ratios in the RGB OSARGs, but the evolutionary sequence of a single initial mass cannot explain the whole range of luminosities (and hence periods) observed. We have to consider a mass distribution along the ridges in the PL relations. Soszyński et al. (2007) and Dziembowski & Soszyński (2010) used isochrones of several ages for the relations between mass and luminosity. Here, we take a more general procedure to obtain the relation be-

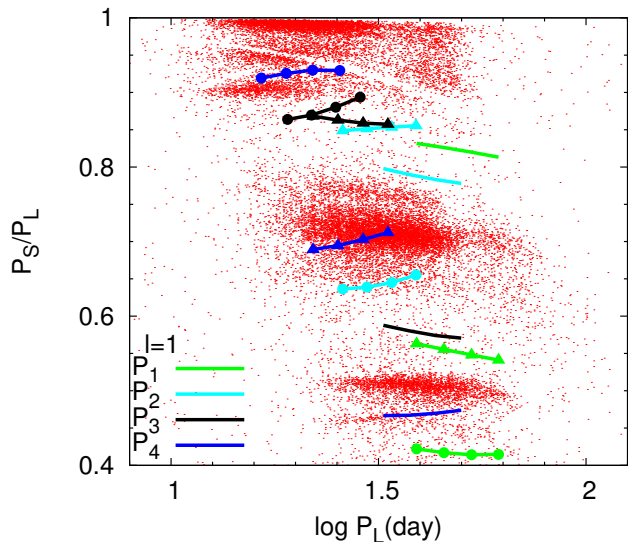


Figure 6. The same as 4 but for period ratios of nonradial dipole ($l = 1$) p-modes, p_1 – p_4 to radial modes of $1.1M_{\odot}$ models. Lines (color coded as indicated) without symbols, with triangles, and with circles indicate period ratios to radial first (1O), second (2O), and third overtones (3O), respectively.

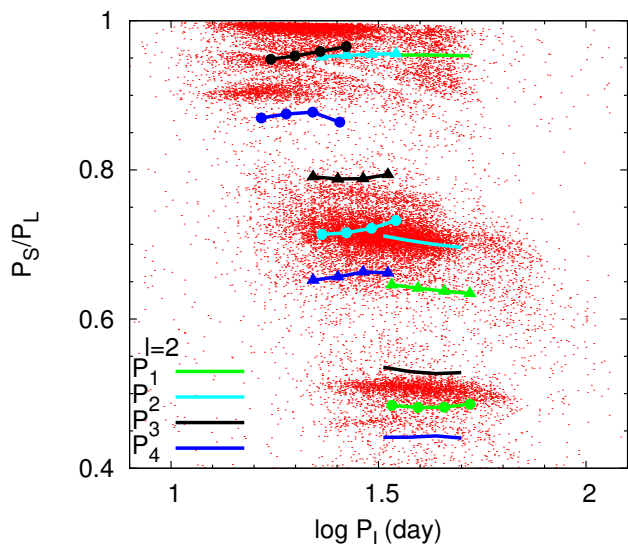


Figure 7. The same as Fig. 6 but for nonradial quadrupole ($l = 2$) p-modes, p_1 – p_4 .

tween mass and luminosity, using the observed PL relations, in particular sequence b_3 .

In order to compare with theoretical relations we have converted the period-magnitude relations shown in Fig. 2 to period-luminosity relations in the following way: K and J magnitudes of each star are obtained from 2MASS photometry data, bolometric corrections for the K magnitudes

$$BC_K = 0.72 + 2.65(J - K) - 0.67(J - K)^2 \quad (3)$$

(Bessell & Wood 1984) are applied, and the LMC distance modulus, 18.54 [mag] (Tabur et al. 2010) is adopted.

For each initial mass we adopt the luminosity range such that the theoretical period-luminosity relation lies within the ‘band’ of sequence b_3 as shown by solid lines in Fig. 8. The boundary of sequence b_3 has been determined as follows. First we chose stars bounded by $1.3 \log P + 1.28 \leq \log L/L_{\odot} \leq 1.3 \log P + 1.51$ and $2.7 \leq \log L/L_{\odot} \leq 3.4$ (dashed red lines in Fig. 8) as tentative members of b_3 . Then we calculated cumulative numbers as a function of period in each luminosity bin and normalized it to unity at the longest period considered. We name this as the normalized cumulative fraction $\Phi_L(P)$ (an example is shown in the bottom panel of Fig. 8). We regard the width of the sequence b_3 at a given luminosity is bounded by periods where $\Phi_L(P) = 0.05$ and 0.95 (dotted lines in the bottom of Fig. 8). We determine such boundaries for each luminosity bin and taking means with adjacent luminosity bins to obtain a smooth curve, as shown by the black solid line in the top panel of Fig. 8.

Using thus obtained boundary for the sequence b_3 , we have determined the luminosity range for each mass. An example is shown in the top panel of Fig. 8. The two blue lines show period to luminosity relations for radial 3O and nonradial $p_4(l = 1)$ modes of $1.1M_{\odot}$ evolutionary models. We adopt the appropriate luminosity range for the mass such that the both lines are within the boundary of b_3 ; the part is indicated by solid lines.

Similarly, we have determined luminosity ranges for models with initial masses of 0.9, 1.0, 1.2, 1.3 and $1.4M_{\odot}$. Fig. 9 compares thus obtained theoretical period-luminosity relations (top panel) and period to period-ratio relations (bottom panel) with observations. This figure demonstrates that our models reproduce the characteristic distributions of RGB OSARGs in the PL and Petersen diagrams quite well. Our models for the RGB OSARGs consist of the three radial overtones and the two nonradial $p_4(l = 1)$, and $p_2(l = 2)$ modes in the evolutionary models having masses between 0.9 and $1.4M_{\odot}$: each mass contributes only in the corresponding appropriate luminosity range. Some other nonradial modes may be involved because clumps in the period-ratios and ridges in the PL plane are broad. We note that the need of different masses for different luminosity ranges comes from the fact that the PL relation of a single mass has a inclination slightly different from the observed one.

The relation between the central value of the luminosity range and mass can be expressed as an empirical formula

$$\log L/L_{\odot} = 0.91(M/M_{\odot}) + 2.05 \quad (4)$$

obtained by a least square fitting. We note that the mass-luminosity relation given in this equation corresponds to ages ranging from about 12.7 Gyr ($0.9M_{\odot}$) to 2.6 Gyr ($1.4M_{\odot}$); indicating massive stars are younger than less massive ones. This means that our mass-luminosity relation is significantly different from isochrone relations.

Dziembowski & Soszyński (2010) argued that pulsations in OSARGs should be excited stochastically by turbulent convection because the run of the scaled optimal frequency ν_{\max} is consistent with the frequencies of sequences b_2 and b_3 , where ν_{\max} is defined as

$$\nu_{\max} = \frac{L_{\odot}}{L} \frac{M}{M_{\odot}} \left(\frac{T_{\text{eff}}}{T_{\text{eff}\odot}} \right)^{3.5} \times 3050 \mu\text{Hz}. \quad (5)$$

Amplitude is maximum at the frequency ν_{\max} in solar-like oscillations excited stochastically by turbulent convec-

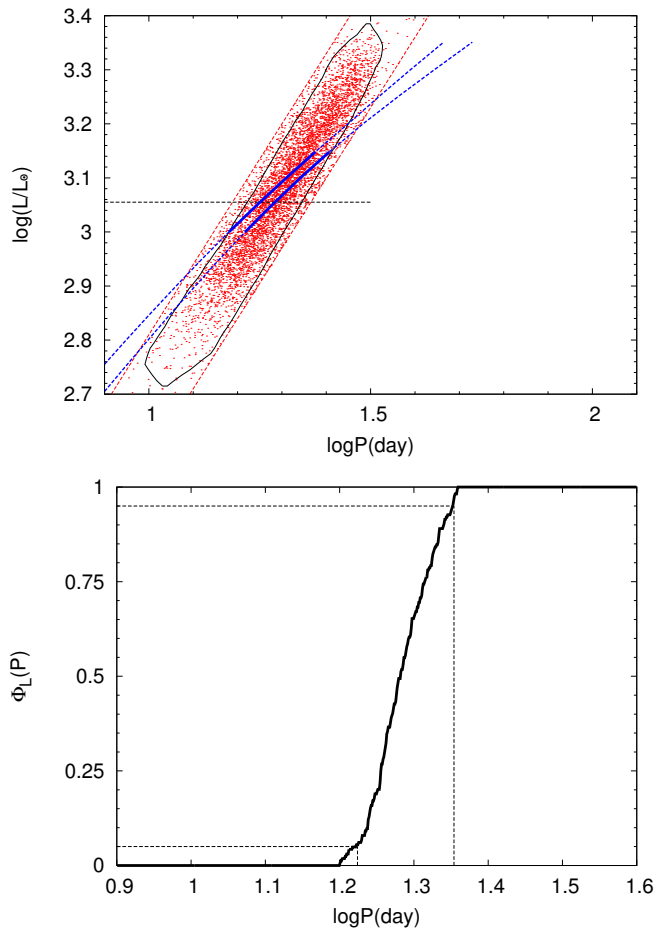


Figure 8. The top panel shows period to luminosity relation obtained from only stars around sequence b3 (red points; see text for how these stars are chosen). The black solid line is the quantitative boundary of the sequence b3 defined using the cumulative distribution function, an example of which is shown in the bottom panel. Dashed (and partially solid) blue lines are relations for the radial 3O and nonradial $p_4(l=1)$ modes of $1.1M_\odot$. The luminosity range adopted for the mass is shown by the part of solid lines. The bottom panel shows a cumulative number of stars in a luminosity bin at $\log L = 3.06$. It is normalized to unity at the longest period is named as $\Phi_L(P)$. We have determined boundary of the sequence b3 by assuming that stars lay in the period range where $0.05 \leq \Phi_L(P) \leq 0.95$; i.e. the range bounded by dotted lines for the luminosity.

tion. The relation was first obtained by Kjeldsen & Bedding (1995), scaling the frequency at maximum power of the solar oscillations. We plot in Fig. 9 (top panel; black dotted line) the run of $1/\nu_{\max}$, the optimal period for the stochastic excitation, calculated using equation (4) and corresponding effective temperature at each luminosity. Also plotted for comparison (cyan dotted line) is the run of $1/\nu_{\max}$ calculated by using the evolutionary track of the $1.1M_\odot$ model with $(Z, \alpha) = (0.004, 1.5)$. For both of the cases, $1/\nu_{\max}$ goes through roughly middle of the PL relations of OSARGs. This suggests, in agreement with Dziembowski & Soszyński (2010), that pulsations in OSARGs are stochastically excited by turbulent convection, and hence kin to the solar-like oscillations observed in

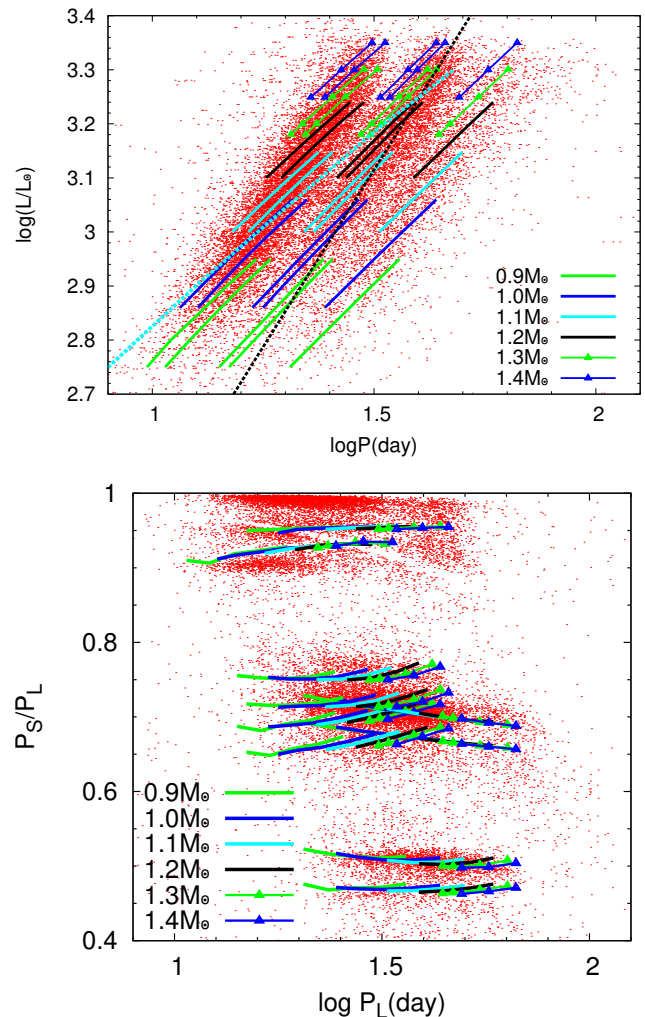


Figure 9. Our best models are compared in the period-luminosity plane (top panel) and in the period vs period-ratio plane (bottom panel) with RGB OSARGs in the LMC. Our theoretical relations include radial first to third overtones and the dipole $p_4(l=1)$ mode and the quadrupole $p_2(l=2)$ mode in models with masses in the range $0.9 \leq M/M_\odot \leq 1.4$. The luminosity range of each mass is determined by fitting with the observed b3 sequence as illustrated in Fig. 8. Black dotted line in the top panel shows the scaled relation $1/\nu_{\max}$ given by equation (5) using the mass to mean luminosity relation given in equation (4) and the corresponding effective temperature. Cyan dotted line shows $1/\nu_{\max}$ computed using the evolutionary track of the $1.1M_\odot$ model with $(Z, \alpha) = (0.004, 1.5)$.

many less luminous red-giants by CoRoT and Kepler (e.g., De Ridder et al. 2009; Bedding et al. 2010). The similarity is also discussed in e.g., Soszyński et al. (2007); Tabur et al. (2010).

5 DISCUSSION

5.1 Effects of metallicity and mixing-length

In our analyses discussed in the previous sections we have adopted a set of parameters $(Z, \alpha) = (0.01, 1.5)$, where

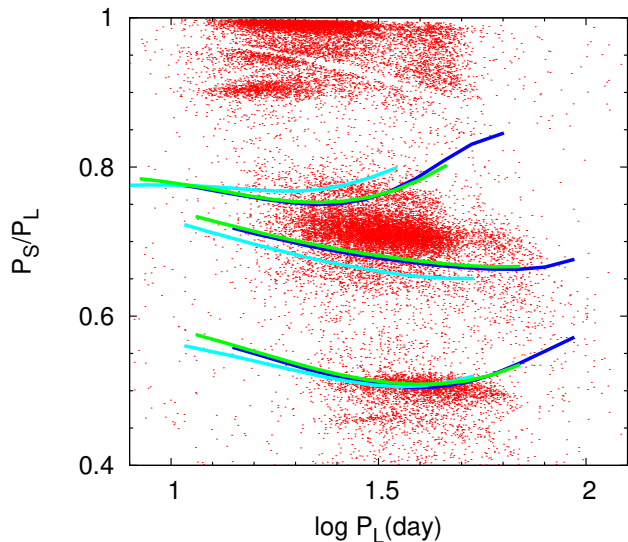


Figure 10. The same as Fig. 5 but including models with (Z, α) different from our standard values. Blue lines are for the standard models (i.e., the same as in Fig. 5), cyan lines are for models with a low metallicity ($Z = 0.004$), and green lines for models with a longer mixing length ($\alpha = 1.8$).

Z is the heavy element abundance and α is the ratio of mixing-length to pressure scale height. We examine here the effect of different choices of (Z, α) . Fig. 10 compares the period/period-ratio relations of radial modes (3O/1O, 2O/1O, and 3O/2O) for the standard set $(Z, \alpha) = (0.01, 1.5)$ with the $(Z, \alpha) = (0.004, 1.5)$ and $(0.01, 1.8)$ cases for $1.1M_{\odot}$ models in the luminosity range $2.7 \leq \log L/L_{\odot} \leq 3.35$. This figure shows that changing metallicity or mixing length hardly changes period ratios, although periods themselves shifts considerably. (Similar results were obtained for different masses in a range of $0.9 \leq M/M_{\odot} \leq 1.4$.)

The period shifts are caused by changes in radius; lower Z or higher α makes the radius smaller (and hence the period shorter) at a given luminosity due to more efficient energy transport. To have the same period we have to adopt a slightly smaller mass compared to our standard case. Although appropriate mass ranges might shift slightly, our mode identifications for the period-luminosity sequences b_1 to b_3 are not affected by changing metallicity or mixing-length.

5.2 Connection to the solar-like oscillations in G/K giants

Another fact supporting the stochastic excitation of OSARG pulsations may be found in the period- M_K diagram shown by Tabur et al. (2010) which shows the sequence of solar-like oscillations in G/K giants extends toward the place where OSARGs are located. The left panel of Fig. 11 is a similar diagram, which shows the relation between luminosity and the period at the maximum amplitude ($1/\nu_{\max}$) for red-giants in the Galactic open clusters NGC 6791 and NGC 6819 obtained by Basu et al. (2011) from Kepler data. The difference between NGC 6791 (squares) and NGC 6819 (triangles) comes from a difference in the range of stel-

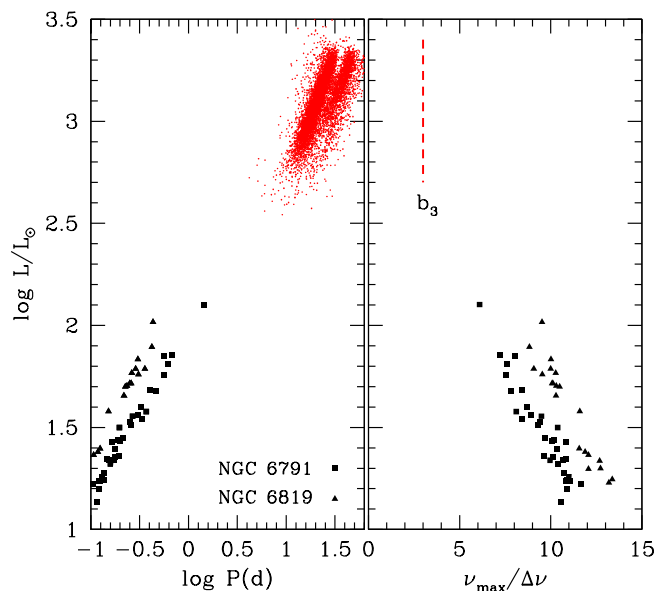


Figure 11. Pulsation properties of OSARGs compared with solar-like oscillations of open cluster giants in NGC 6791 and NGC 6819 obtained by Basu et al. (2011) from Kepler data. *Left panel* shows luminosity versus period ($1/\nu_{\max}$) of maximally excited mode in the solar-like oscillations of the cluster giants, and period-luminosity relations of OSARGs in the LMC (red dots), where only the primary period for each OSARG is plotted. *Right panel* shows luminosity versus $\nu_{\max}/\Delta\nu$ which gives the approximate number of radial nodes for the maximally excited mode in the cluster giants. The vertical dashed line indicates the number radial nodes of radial 3O mode which we fit to the sequence b_3 .

lar masses; stars in the latter cluster systematically more massive ($\sim 1.6 - 2.0M_{\odot}$) than those in the former cluster ($\sim 1.0 - 1.5M_{\odot}$) according to the seismic mass determinations by Basu et al. (2011). Also plotted are period-luminosity relations of our sample RGB OSARGs (red dots).

The right panel of Fig. 11 shows $\nu_{\max}/\Delta\nu$ of the solar-like oscillations in the cluster giants, where $\Delta\nu$ means the large separation. The value of $\nu_{\max}/\Delta\nu$ is roughly equal to the number of radial nodes in the maximally excited mode. The vertical dashed line indicate the number of radial node (3) for the radial third overtone mode which we fit to the sequence b_3 of OSARGs. The radial order of the modes excited in the solar-like oscillations decreases with increasing luminosity, which is consistent with the fact that only low-order modes are excited in the OSARGs.

These diagrams indicate that the properties of OSARGs can be understood as the high luminosity (and hence long period) extension of the solar-like oscillations in G/K giants; in other words OSARGs are likely excited stochastically by turbulent convection.

6 SUMMARY

We studied period-luminosity relations and period ratios of RGB OSARGs in the LMC, and found that these relations can be explained by radial first to third overtones and non-

radial $p_4(l=1)$ and $p_2(l=2)$ modes in evolving red-giant models having masses between about 0.9 and $1.4M_{\odot}$ for our standard parameters of $(Z, \alpha) = (0.01, 1.5)$. Although different choices for the parameters would shift the mass ranges, mode identifications are not affected because the period ratios hardly depend on these parameters. The sequence b_1 is fitted by radial 1O, b_2 by radial 2O and nonradial $p_2(l=2)$, and b_3 by radial 3O and nonradial $p_4(l=1)$ modes. The reason why only the two nonradial modes are observed is not clear.

The scaled ν_{\max} of solar-like oscillations evaluated with our model parameters goes through roughly the middle of the three ridges populated by RGB OSARGs in the period-luminosity plane. In addition, the period-luminosity relations look like a high-luminosity extension of the solar-like oscillations recently detected by the Kepler satellite in G/K giants of the open clusters NGC 6791 and NGC 6819. These facts strongly suggest that pulsations in OSARGs are stochastically excited by turbulent convections.

ACKNOWLEDGMENTS

This publication makes use of data products from the Two Micron All Sky Survey, which is a joint project of the University of Massachusetts and the Infrared Processing and Analysis Center/California Institute of Technology, funded by the National Aeronautics and Space Administration and the National Science Foundation.

REFERENCES

- Alexander D. R., Ferguson J. W., 1994, *ApJ*, 437, 879
 Basu S., Grundahl F., Stello D., Kallinger T., Hekker S., Mosser B., García R. A., Mathur S., Brogaard K., Bruntt H., *et al.*, 2011, *ApJ*, 729, L10
 Bedding T.R., Huber D., Stello D., Elsworth Y.P., Hekker S., Kallinger T., Mathur S., Mosser B., *et al.*, 2010, *ApJ*, 713, L176
 Bessell M.S., Wood P.R., 1984, *PASP*, 96, 247
 Cioni M.-R. L., Marquette J.-B., Loup C., Azzopardi M., Habing H. J., Lasserre T., Lesquoy E., 2001, *A&A*, 377, 945
 Cox J.P., 1980, *Theory of stellar pulsation*. Princeton University Press
 De Ridder J., Barban C., Baudin F., Carrier F., Hatzes A.P., Hekker S., Kallinger T., Weiss W.W., Baglin A., Auvergne M., Samadi R., Barge P., Deleuil M., 2009, *Nature*, 459, 398
 Dupret M.-A., Belkacem K., Samadi R., Montalbán J., Moreira O., Miglio A., Godart M., Ventura P., Ludwig H.-G., Grigahcène A., Goupil M.-J., Noels A., Caffau E., 2009, *A&A*, 506, 57
 Dziembowski W.A., Soszyński, I., 2010, *A&A*, 524, A88
 Fox M. W., Wood. P. R., 1982, *ApJ*, 259, 198F
 Iglesias, C. A., Rogers, F. J., 1996, 464, 943
 Ita Y., Tanabé T., Matsunaga N., Nakajima Y., Nagashima C., Nagayama T., Kato D., Kurita M., Nagata T., Sato S., Tamura M., Nakaya H., Nakada Y., 2004, *MNRAS*, 347, 720
 Kiss L.L., Bedding T.R., 2003, *MNRAS*, 343, L79
 Kjeldsen H., Bedding T.R., 1995, *A&A*, 293, 87
 Nicholls C.P., Wood P.R., Cioni M.-R.L., Soszyński I., 2009, *MNRAS*, 399, 2063
 Nicholls C.P., Wood P.R., Cioni M.-R.L., 2010, *MNRAS*, 405, 1770
 Noda, S., Takeuti, M., Abe, F., Bond, A., Dodd, R.J., Hearnshaw, J.B., Honda, M., Honma, M., Jugaku, J., Kan-ya, Y., *et al.*, 2004, *MNRAS*, 348, 1120
 Paxton, B., Bildsten, L., Dotter, A., Herwig, F. Lesaffre, P., Timmes, F., 2011, *ApJS*, 192, id.3
 Reimers D., 1975, *Mem. Soc. Roy. Sci. de Liege*, 8, 369
 Saio, H., Cox, J. P., 1980, *ApJ*, 236, 549
 Saio, H., Winget, D. E., Robinson, E. L., 1983, *ApJ*, 265, 982
 Soszyński I., 2007, *ApJ*, 660, 1486
 Soszyński I., Udalski A., Kubiak M., Szymański M., Pietrzyński G., Zebruń K., Szewczyk O., Wyrzykowski L., 2004, *AcA*, 54, 129
 Soszyński I., Dziembowski W.A., Udalski A., Kubiak M., Szymański M.K., Pietrzyński G., Wyrzykowski L., Szewczyk O., Ulaczyk K., 2007, *AcA*, 57, 201
 Soszyński I., Udalski A., Szymański M., Kubiak M., Pietrzyński G., Wyrzykowski L., Szewczyk O., Ulaczyk K., Poleski R., 2009, *AcA*, 59, 239
 Tabur V., Bedding T.R., Kiss L.L., Giles T., Derekas A., Moon T.T., 2010, *MNRAS*, 409, 777
 Wood, P.R., *et al.* (MACHO team) 1999, in: *IAU Symp.* 191, *Asymptotic Giant Branch Stars*, Eds. T. Le Bertre, A. Lébre, and C. Waelkens (San Francisco: ASP), p. 151.
 Wood P. R., Olivier E. A., Kawaler S. D., 2004, *ApJ*, 604, 800
 Xiong D. R., Deng L., 2007, *MNRAS*, 378, 1270